JACS
JOURNAL OF THE AMERICAN CHEMICAL SOCIETY

Article

pubs.acs.org/JACS

Mechanism of the Photoinduced Uncaging Reaction of Puromycin Protected by a 6-Nitroveratryloxycarbonyl Group

Jörg Kohl-Landgraf,[†] Florian Buhr,[‡] Daniel Lefrancois,[§] Jan-Michael Mewes,[§] Harald Schwalbe,[‡] Andreas Dreuw,[§] and Josef Wachtveitl*,[†]

[†]Institute of Physical and Theoretical Chemistry, Goethe University Frankfurt, Max-von-Laue Str. 7, 60438 Frankfurt/Main, Germany

[‡]Institute of Organic Chemistry and Chemical Biology, Goethe University Frankfurt, Max-von-Laue Str. 7, 60438 Frankfurt/Main, Germany

[§]Interdisciplinary Center for Scientific Computing, Ruprecht-Karls University, Im Neuenheimer Feld 368, 69120 Heidelberg, Germany

Supporting Information

ABSTRACT: The cleavage of a photolabile nitroveratryloxycarbonyl protecting group, which is widely used as caging group, was studied by femtosecond transient absorption spectroscopy in the visible and infrared spectral range and by flash-photolysis experiments on the longer time scale. On the basis of quantum-chemical calculations it is shown that directly after excitation, triplet absorption that is not part of the reactive pathway dominates the transient spectrum and that the molecules following the triplet pathway are trapped in a nonreactive triplet state. By contrast, photolysis proceeds from the singlet manifold. Therefore, trapping in the triplet state lowers the quantum yield of the process for this compound compared with other *o*-nitrobenzyl protecting groups. With our integrated approach of time-resolved UV and IR measurements and calculations, we can characterize the entire uncaging mechanism and identify the most relevant intermediate states along the reaction pathway. The final uncaging is accomplished within 32 μs.

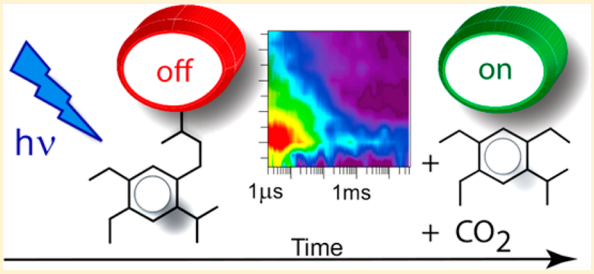

INTRODUCTION

Caged compounds are chemically or biologically active molecules that are deactivated by coupling to a protecting group, the so-called cage, which can be removed by application of various external triggers. In the case of photolabile protecting groups, these cages provide a harmless and highly specific method to initiate chemical or biological processes.[1−5] A selection of recent reviews is provided in refs 6−10. Cages of the *o*-nitrobenzyl (oNB) type have come more and more into the focus of interest throughout the last decades. Especially the nitroveratryloxycarbonyl (NVOC) group, which is of the 4,5-dimethoxy-2-nitrobenzyl (DMNB) type, is one of the most frequently used cages.[11−13] The requirements for a cage to be a valuable tool in biology are good water solubility and a high uncaging yield in combination with fast release of the protected molecule. In addition, light absorption, which initiates the uncaging mechanism of the compound, should be in a range where the protected molecule does not absorb in order to circumvent harmful side reactions such as lesions. Furthermore, the cage should exhibit low cytotoxicity for in vivo applications.

The effect of light on oNB was first mentioned by Ciamician and Silber more than a century ago, and its capability as photoreactive cage has been known since the 1960s.[14−16] The photochemical behavior of oNB caging groups has been studied intensively throughout the last years, indicating their high potential and relevance as regulatory tools.[17,18] However, these compounds usually absorb in the UV range, which reduces their applicability in living cells. In contrast, substitution with electron-donating groups on the benzene ring induces a bathochromic shift that results in an absorption maximum around 350 nm.[19,20] One example of this class of molecules are the DMNB compounds mentioned above, where two methoxy groups are attached on the benzene ring, but 4,5-methylenedioxynitrobenzyl also shows that effect. Theoretical studies comparing oNB and its substituted derivatives show that the singlet states are not shifted and that it is a change in the oscillator strengths that causes the change in the absorption spectrum.[21] The uncaging reaction of oNB compounds after photoexcitation is generally believed to proceed by the reaction mechanism proposed by Schaper et al.[21] (Scheme 2). Upon absorption of a photon, an *aci*-nitro intermediate **1** is formed by hydrogen transfer from the methylene group to the *o*-nitro group via either the singlet or triplet manifold after ultrafast intersystem crossing (ISC). As a result of the increased double-bond character between the nitrogen and the benzene ring in the initial *aci*-nitro form **1**, a high rotational barrier exists that allows for the formation of the cyclic intermediate **4** only via

Received: October 16, 2013
Published: February 11, 2014

   dx.doi.org/10.1021/ja410594y | *J. Am. Chem. Soc.* 2014, 136, 3430−3438

Scheme 1. Constitution of NVOC−Puromycin

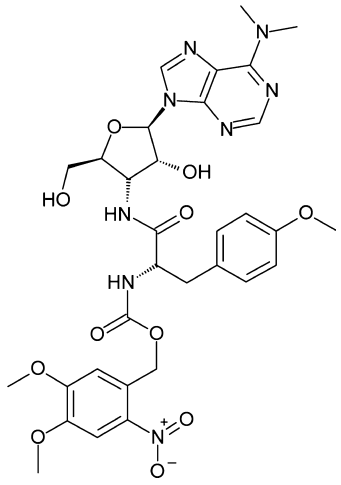

preceding proton-transfer reactions forming **3** from **1**. However, recent calculations have also shown that in the triplet state of **1** the *aci*-nitro group can easily rotate.[22] Via the transition state **5**, the decay of the cyclic intermediate **4** finally leads to the formation of nitrosobenzene **6** and eventually to the release of the deprotected compound **7** and CO_2. For DMNB compounds it was found that molecular oxygen quenches a triplet state with charge-transfer character, which does not contribute to the formation of the *aci*-nitro intermediate in the singlet state.[19] The triplet state in DMNB compounds exhibits a dominant contribution in the transient absorption spectrum on the low nanosecond time scale, and it usually decays within 0.4 to 2 μs.[17] In contrast, the absorption feature of the *aci*-nitro intermediate in the singlet state shows only a minor contribution around 410 nm. Its decay occurs in the range from microseconds to milliseconds, depending on the substituents and solvent.[17] The decay results in the formation of nitrosobenzenes **6** and **7** and constitutes the rate-limiting step for the uncaging process. It was found that the uncaging quantum yield of DMNB compounds is about 1 order of magnitude lower than the quantum yield of compounds without substituents on the benzene ring: whereas for unsubstituted oNB an uncaging yield of about 10% was found, a yield in the range of 1% was obtained for compounds protected with a DMNB group.[20,23]

NVOC was introduced as a caging group by Patchornik et al. in 1970.[12] Like other DMNB compounds, it provides the desired bathochromic absorbance compared with unsubstituted oNB. Even though NVOC is probably the most popular photolabile protecting group,[11] we could not find studies on the photodynamics of this compound, but analogies to the spectral properties of other DMNB compounds are evident. Early studies on the uncaging mechanism showed that the reaction is accompanied by a decarboxylation, which can be used as an indicator for the amount of released molecules.[16] However, to the best of our knowledge, no studies on the ultrafast dynamics of either NVOC or other DMNB derivatives in the picosecond regime after photoexcitation have been reported.

Here we report on caged puromycin with a photolabile NVOC protecting group (Scheme 1). Puromycin is an antibiotic that interferes with the translation process at the ribosome, where it binds codon-unspecifically to replace the 3′ end of a tyrosyl-tRNA at the ribosomal A-site and facilitates the release of the nascent chain caused by the stability of its amide bond against hydrolysis.[24−26] If many puromycin molecules are applied to stalled ribosomal nascent chain complexes in a concerted manner, as is possible when the puromycin molecules are protected with a fast removable photolabile group, the kinetics of post-translational folding events can be investigated.

With our femtosecond transient absorption measurements in the visible spectral range, we demonstrate that the spectral features described earlier for DMNB 20 ns after excitation are in fact also formed for the NVOC protecting group on a picosecond time scale and are caused mostly by absorptions of the *aci*-nitro intermediate in the triplet state.[17] These features obscure the weak contributions of the *aci*-nitro intermediate in the singlet state in that time regime. To substantiate that a photoreaction in the singlet state also takes place, we performed

Scheme 2. Proposed Uncaging Mechanism of NVOC−Puromycin According to Schaper et al.[21]

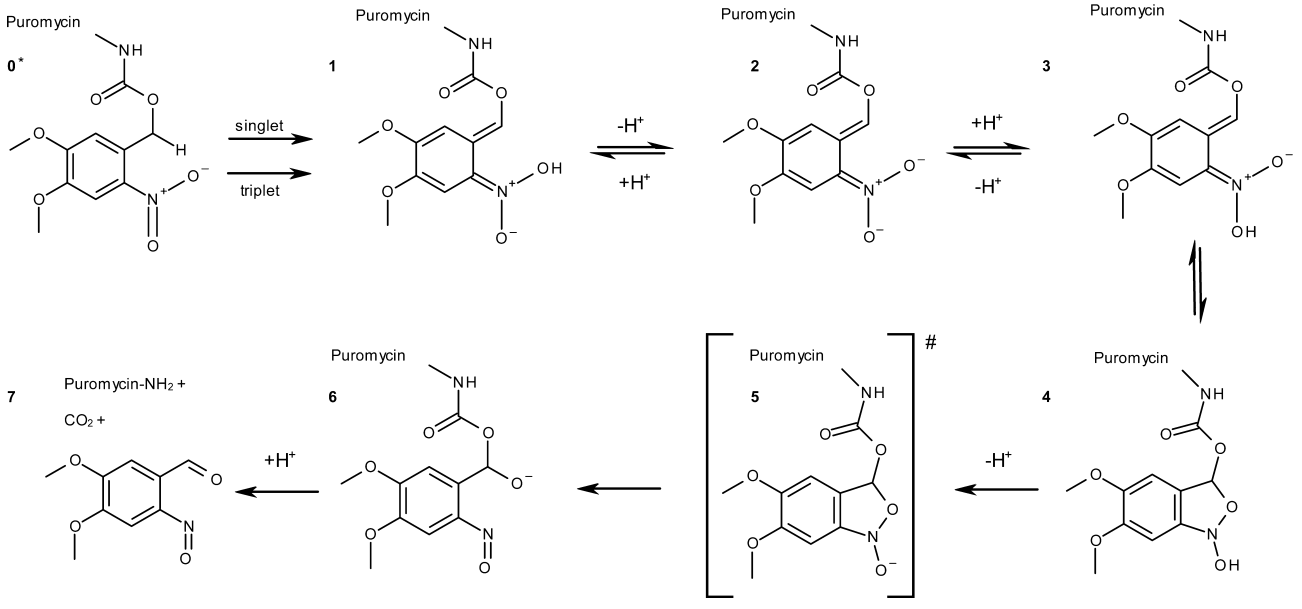

dx.doi.org/10.1021/ja410594y | J. Am. Chem. Soc. 2014, 136, 3430−3438

transient absorption measurements in the infrared spectral range that allowed us to identify characteristic vibrational modes of the singlet *aci*-nitro intermediate appearing after the initial cooling processes in the range of a few picoseconds. In a flash photolysis experiment, we demonstrate that the triplet state has a lifetime smaller than 2 μs and that the final release of the puromycin occurs within 32 μs. To identify the intermediates along the reaction pathway, their spectra were calculated by means of time-dependent density functional theory (TDDFT), and the influence of water on the relative energies of these intermediates was studied.

In summary, we can identify the complete photoinduced reaction mechanism and the intermediates involved, providing evidence that some intermediates that have been proposed earlier for oNB do not appear along the photolysis reaction of NVOC–puromycin.[21] To the best of our knowledge, this is the first experimental study covering the whole reaction mechanism of a DMNB compound from the femtosecond time regime until the final uncaging reaction.

MATERIALS AND METHODS

Synthesis. The synthesis of NVOC–puromycin is described in the Supporting Information.

Femtosecond UV-Pump/Visible-Probe Experiments. The transient absorption measurements were carried out in pump/probe configuration. The femtosecond-laser source was a Ti:Sa chirped pulse regenerative amplifier with a central output wavelength of 775 nm, a 1 kHz repetition rate, and a pulse width of about 170 fs. For the excitation pulses, the sum frequency of nonlinear optical parametric amplifier (OPA) pulses at 640 nm and a small fraction of the fundamental pulses was generated, resulting in 350 nm pulses with an energy of about 75 nJ. The probe light was created by focusing fundamental pulses into a CaF_2 plate, where supercontinuum white light was generated. The polarizations of the two pulses were aligned in such a way that the angle between them was 54.7° to eliminate anisotropic effects. The sample was diluted in dimethyl sulfoxide (DMSO) to a concentration of 2.3 mM and put into a cuvette with 1 mm sample thickness, resulting in an optical density of 1.3 at 350 nm. The water content of the solution was about 2%. This content was estimated by determining the height of the 1645 cm^{-1} water absorption band in an FTIR measurement of the sample (see the Supporting Information). During the measurement, the cuvette was moved continuously to provide a variation of the excitation volume. The temporal resolution was in the range of 180 fs.

Femtosecond UV-Pump/IR-Probe Experiments. The excitation pulses for the transient absorption measurement in the infrared were created as described above. The probe light was generated in a two-step OPA configuration with subsequent difference frequency generation.[27] In the range from 1450 to 1770 cm^{-1}, four measurements were carried out in different frequency regions, and the transient spectra were subsequently merged. The excitation energy was in the range of 70 nJ. The sample was diluted in DMSO (about 2% water content as mentioned above) to a concentration of 35 mM and placed between two CaF_2 plates that were separated by a 50 μm thick Teflon spacer, resulting in an absorbance of 1 around 350 nm. In the same way as in the visible-probe experiment, the angle between the polarizations of the pump and probe pulses was set at the magic angle. The global analysis was performed from 0.5 ps onward, where the signal was free of nonlinear contributions from the coherent artifact. The temporal resolution was in the range of 250 fs.

Flash Photolysis. The sample was diluted in a 1:1 mixture of DMSO and water to a concentration of 60 μM and put into a 3 × 10 mm cuvette. The pulse energy of about 40 mJ centered around 355 nm was generated in a Spitlight 600 laser. Ten shots were averaged at a specific wavelength before the sample was exchanged.

Quantum-Chemical Calculations. All of the calculations were performed using the program packages ORCA[28] and Q-Chem 4.0.[29] For the theoretical investigation of the uncaging mechanism after *aci*-nitro formation, 4,5-dimethoxy-2-nitrobenzyl acetate was used as a molecular model, since the detailed structure of the protected group does not play a role for the general uncaging mechanism of DMNB protecting groups. It is clear that after uncaging of the carbamate, its hydrolysis occurs and the puromycin is released. However, this step was not theoretically investigated. The ground-state geometries of all possible intermediates were optimized at the theoretical levels of DFT/B3LYP[30,31] and spin-component-scaled second-order Møller–Plesset perturbation theory (SCS-MP2),[32,33] for which the resolution-of-the-identity approximation was exploited.[34] In all of the calculations, the cc-pVTZ basis set and the corresponding density fitting basis were used. To account for solvent effects, aqueous solution was simulated using the conductor-like screening model (COSMO)[35] within all of the reported calculations by default. UV/vis spectra of all intermediates were computed using TDDFT[36] in combination with the standard B3LYP exchange–correlation (xc) functional. For the calculation of static absorption spectra, the standard B3LYP functional is sufficient, since it reproduces optically allowed states, which correspond mainly to $\pi\pi^*$ excited states, with good accuracy. For the calculation of potential energy surfaces, however, the PBE0 xc functional turned out to yield superior results, which were found to agree with those of RI-CC2.[22]

RESULTS

Steady-State Spectroscopy. The spectrum of NVOC–puromycin (red area in Figure 1 bottom) shows an absorption maximum around 350 nm. The absorbance becomes stronger toward lower wavelengths, with a maximum around 278 nm that shows a weak shoulder around 300 nm. The spectrum of pure NVOC (black curve) shows the typical red-shifted absorption known for DMNB compounds, in addition to which a weaker shoulder around 300 nm appears.[21] The peak around 278 nm does not appear in the absorption spectrum of pure NVOC (black line) but is seen in the spectrum of puromycin (blue line). It originates from the adenosine moiety, since it is in the typical absorption region of nucleobases. It is obvious that the spectrum of NVOC–puromycin is almost a superposition of the spectra of its components. Irradiation of the caged compound with UV light at 365 nm leads to a reduction of the specific NVOC absorbances at 300 and 350 nm and at the same time to a slight rise around 410 nm due to the formation of the nitroso product (Figure 1 top). Further product absorbances appear below 300 nm.

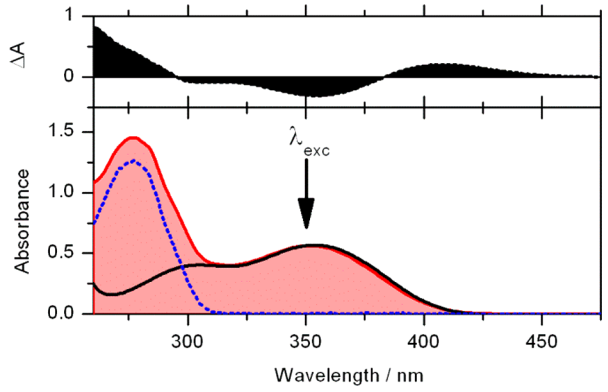

Figure 1. (bottom) Absorption spectrum of caged NVOC–puromycin (red area). In addition, scaled absorption spectra of NVOC (black curve) and puromycin (blue curve) are shown. The arrow indicates the spectral position of the excitation pulses used in the femtosecond transient absorption experiments. (top) Difference spectrum after UV irradiation of NVOC–puromycin, represented by the black area.

dx.doi.org/10.1021/ja410594y | J. Am. Chem. Soc. 2014, 136, 3430–3438

Figure 2 shows an IR difference spectrum of the caged compound and the nitroso product, where positive peaks mark

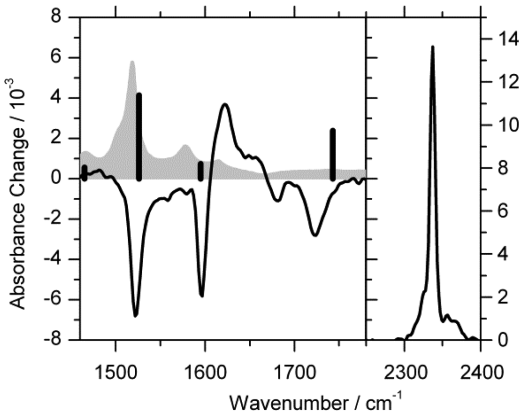

Figure 2. (left) IR difference spectrum of NVOC−puromycin and the photoproduct (black curve). In addition, a scaled absorption spectrum of NVOC is shown (gray area). The black bars represent the calculated spectrum of NVOC in the gas phase. (right) Solubilized CO_2 can be observed around 2340 cm^{-1}.

the positions of product bands formed after cleavage of the caging group and negative ones the bleached modes from the parent caged puromycin. Upon UV irradiation, a series of electron and proton transfer reactions take place that lead to free puromycin and to the formation of the nitroso product, respectively. Since the constitution of the puromycin remains unchanged during this reaction, the difference spectrum originates mostly from changes within the NVOC cage. The absorption spectrum of NVOC without puromycin (Figure 2, gray area) verifies that the spectral changes appear mostly in regions of the NVOC main absorptions. The nitroso product has a dominant mode in the region around 1625 cm^{-1} and a weaker one at 1650 cm^{-1}. The bleached modes of the initial NVOC appear around 1520, 1600, and 1725 cm^{-1} and weakly at 1680 cm^{-1}. The most dominant negative contribution in the difference spectrum is the one around 1520 cm^{-1}, which is due to the loss of the NO stretching mode in the nitro group. Further strong features disappear around 1600 and 1625 cm^{-1}, which can be explained by the change in the aromatic ring vibrations with the change in the substitution pattern during the photoreaction. In addition, the difference spectrum in the region around 2340 cm^{-1} is shown (right half), demonstrating the formation of solubilized CO_2 during the uncaging reaction.

Femtosecond UV-Pump/Visible-Probe Experiments. The transient absorption spectrum probing the dynamics in the visible and near-UV range is shown in Figure 3a. Directly after excitation, the spectrum is dominated by a broad featureless positive absorption covering almost the entire probe range up to 300 fs. At longer delay times, a positive band rises around 530 nm that becomes weaker after a few picoseconds in combination with the rise of a signal around 500 nm. In addition, a band around 410 nm increases in intensity. Both components are formed within a few picoseconds and preserve their spectral shape up to 1 ns. A negative absorption feature is apparent in the UV range around 370 nm that appears within the temporal resolution and changes sign at long delay times. In a global fit analysis with a sum of exponential decay functions, three time constants are required to describe the dynamics adequately. This analysis was performed on the data

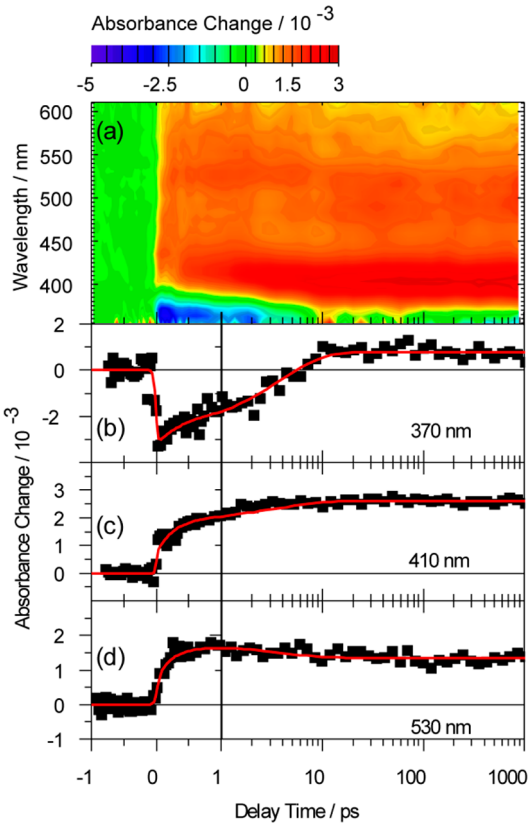

Figure 3. (a) Transient absorption spectrum in the visible spectral range after 350 nm excitation of NVOC−puromycin in DMSO. (b−d) Transients at selected wavelengths with the respective multi-exponential fits.

shown in Figure 3a, where effects due to the chirp of the probe light and dominant contributions of cross-phase modulation of the pump and probe pulses within the solvent were eliminated from the transient spectrum. The respective decay-associated spectra (DAS) of the involved time constants are shown in Figure 4. A 200 fs time constant is in the range of the temporal resolution and describes the rise of the features around 530 and below 430 nm. The DAS of the 3.6 ps time constant shows a

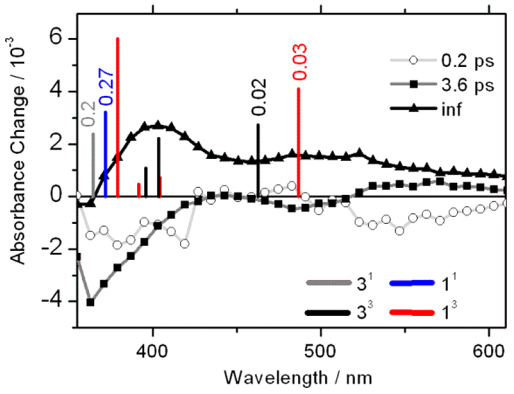

Figure 4. Decay-associated spectra (DAS) of the involved time constants for the transient absorption measurement of NVOC−puromycin in the visible spectral range. In addition, calculated spectra of the *aci*-nitro intermediates are shown as bars. The spectra are arbitrarily scaled with respect to each other for a better representation. Within each spectrum, one oscillator strength is provided as a measure.

dx.doi.org/10.1021/ja410594y | J. Am. Chem. Soc. 2014, 136, 3430−3438

large negative amplitude below 420 nm, a minor negative amplitude around 500 nm, and a small positive amplitude above 520 nm. Therefore, it describes not only the decrease of the negative signal amplitude and the rise of the band around 410 nm but also the shift of the absorption from 530 to 500 nm indicated by its sigmoidal structure. The spectral components around 410 and 500 nm preserved their shapes at long delay times and were therefore modeled with an infinite time constant. In addition, the calculated spectra of the triplet intermediates $\mathbf{1}^3$ and $\mathbf{3}^3$ and the singlet intermediates $\mathbf{1}^1$ and $\mathbf{3}^1$ are shown as columns representing the obtained oscillator strengths. For a better representation, the calculated spectra were scaled independently of each other. All of the intermediates show strong contributions in the region around 400 nm, where compared with the DAS of the infinite time constant also the most prominent positive absorption change can be found. Because of their proximity, a superposition of the spectra of the intermediates is likely in this region. Remarkably, the shift of the absorbance from 530 to 500 nm can also be found in the reddest calculated spectral contributions of the intermediates $\mathbf{1}^3$ and $\mathbf{3}^3$, where a shift of about 25 nm can be observed in going from intermediate **1** to **3**.

Femtosecond UV-Pump/IR-Probe Experiments. To obtain more specific insight into the mechanism on a picosecond time scale, pump/probe measurements in the IR were performed. The transient IR absorption spectrum (Figure 5) was recorded in the range from 1460 to 1760 cm^{-1}. At negative delay times, contributions of the perturbed free induction decay can be observed mainly at 1520 cm^{-1}, indicating the spectral position of dominant bleached ground-state modes. Around a delay time of zero, the coherent artifact dominates the transient spectrum, obscuring direct information on the sample dynamics. At early positive delay times, the transient spectrum contains features of cooling processes, where bleached ground-state modes are accompanied by broad positive absorption bands that decay within a few picoseconds. These bands dominate the spectrum up to a few picoseconds. Toward long delay times, only two positive signals at 1475 and 1545 cm^{-1}, with the strongest one at 1475 cm^{-1}, can be observed, whereas bleached modes remain around 1580 and 1675 cm^{-1} and dominantly around 1520 cm^{-1}. A global fit analysis showed that the data set was best modeled with three time constants. The respective DAS are given in Figure 6. The DAS of the 7.8 ps time constant describes the cooling processes mentioned above, since it shows the typical sigmoidal pattern. At long delay times, the spectral changes are modeled with an infinite time constant, showing that the initially bleached modes remain bleached at 1520, 1580, and at 1675 cm^{-1} whereas the product bands are the same as the ones described above that are present after a few picoseconds. In addition, the DAS of the 3.7 ps time constant appears to have the same spectral features as the 7.8 ps DAS but with opposite sign and slightly shifted maxima and therefore describes early relaxation processes.

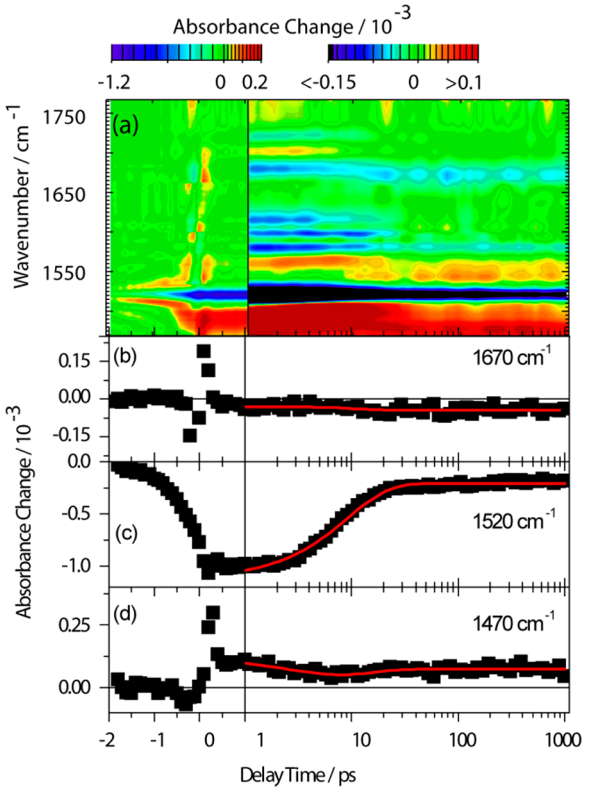

Figure 5. (a) Transient absorption spectrum of NVOC–puromycin in DMSO in the IR spectral range after 350 nm excitation. The linear and logarithmic ranges were scaled independently for a better representation. (b, c) Selected transients.

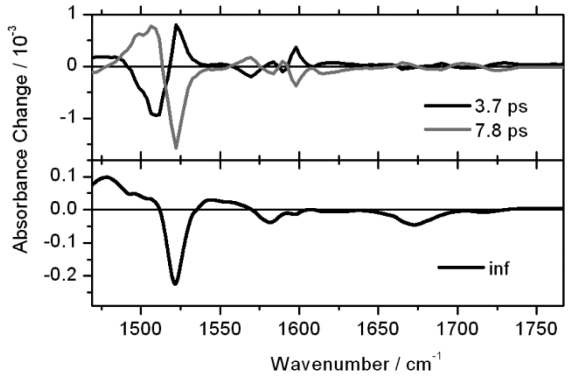

Figure 6. DAS of the transient absorption measurement in the IR spectral range of NVOC–puromycin.

We also probed the dynamics near 2340 cm^{-1} to determine whether an additional ultrafast reaction pathway leading to a decarboxylation exists in the picosecond time range, as is known for *o*-nitrophenyl acetate (oNPA),[22,37,38] but we could not find any traces of solubilized CO_2 within 1 ns, indicating that this ultrafast pathway does not exist for NVOC (see the Supporting Information).

Flash Photolysis. The decay of the *aci*-nitro form into the nitroso product was recorded in a flash photolysis measurement. The obtained transient spectrum is shown in Figure 7. At early times, the spectrum is dominated by a strong absorption around 410 nm that is accompanied by a contribution that stretches out toward longer wavelengths. A comparison of a time slice taken 5 μs after excitation with a scaled time slice taken after about 1 ns in the femtosecond time-resolved measurement (Figure 8) shows that the band around 410 nm also appears in the earlier spectrum whereas the contribution around 500 nm has vanished at the beginning of the flash photolysis measurement. At longer times, the spectrally broad feature disappears, whereas a residual absorption with a maximum around 400 nm remains throughout the investigated time range. A scaled steady-state difference spectrum agrees well with a time slice taken after 1 ms, indicating that the

dx.doi.org/10.1021/ja410594y | J. Am. Chem. Soc. 2014, 136, 3430–3438

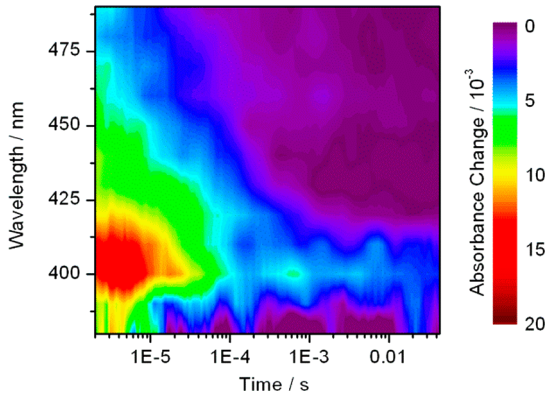

Figure 7. Transient absorption spectrum of the flash photolysis measurement.

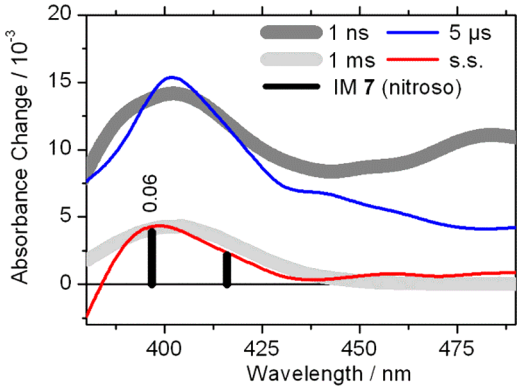

Figure 8. Time slices from the flash photolysis measurement (thin blue and red lines), a scaled time slice from the femtosecond transient absorption measurement (thick dark-gray line), and a scaled steady-state spectrum (thick light-gray line). In addition, the calculated spectrum of the nitroso product **7** is shown.

photoreaction is finished. A fit of the signal at 410 nm using a single-exponential function with a constant offset revealed a time constant of 32 μs (see the Supporting Information). In addition to the difference spectra at various delay times, the calculated spectrum of the nitroso product **7** (Figure 8) reveals remarkably good congruence with the experimental spectrum after 1 ms.

Quantum-Chemical Calculations. The uncaging mechanism of NVOC-caged puromycin (Scheme 2) was investigated using DFT/B3LYP as well as SCS-MP2 in combination with the cc-pVTZ basis set. This study was focused on the processes occurring after the formation of the *aci*-nitro form **1**, since the theoretical investigation of the mechanism of *aci*-nitro formation has been published previously.[22,39] In the calculations, 4,5-dimethoxy-2-nitrobenzyl acetate was used as a smaller molecular model for NVOC–puromycin, since the protected compound has no influence on the uncaging mechanism.

The exact energetic order of the two lowest triplet states of nπ^* and CT character is important for the progress of the uncaging reaction. In analogy to previous results,[22,39] the relaxed geometry of the reactive nπ^* triplet leading to fast uncaging is 0.3 eV higher in energy than the relaxed geometry of the long-lived CT triplet state when aqueous equilibrium solvation using the COSMO model is employed at the DFT/PBE0 level. For less polar solvents and the gas phase, the order of the energies of these minima is reversed.

As first step, the ground-state geometries of all of the possible compounds **1**–**7** as well as all of the transition states connecting them were optimized. All of the identified stationary states were confirmed by calculations of their harmonic frequencies. All of the reported equilibrium structures exhibited only real harmonic frequencies, while the transition states were characterized by one single imaginary frequency representing the motion along the path connecting the two corresponding minima on the potential energy surface.

Starting with the protonation equilibria **1** + H_2O ⇄ **2** + H_3O^+ ⇄ **3** + H_2O, the energetics of the underlying reactions were computed. The total energies of the cage and a solvated water or hydronium ion were added together to obtain the relative energies displayed in Table 1. It turns out that **3** + H_2O is the most stable species, while **1** + H_2O is 12.2 and 13.5 kJ/mol less stable at the DFT/B3LYP and SCS-MP2 levels of theory, respectively. Remarkably, the deprotonated species **2** + H_3O^+ is as much as about 150 kJ/mol less stable and hence is very unlikely to be formed at room temperature. If thermal equilibrium of these three species is assumed, their Boltzmann populations correspond to 99.99% **3**, less than 0.01% **1**, and no **2** ($\sim 10^{-26}$ %) at the DFT/B3LYP and SCS-MP2 levels. Although the energy of **2** is probably too high because of limitations of the applied solvation model and a more sophisticated theoretical treatment would be required to obtain more accurate energetics,[40] it still appears unlikely that **3** is formed according to the protonation/deprotonation mechanism displayed in Scheme 2 since this would require the extremely unlikely formation of **2**. This on one hand either supports the earlier finding that **3** is already formed in the triplet manifold[22] or on the other hand suggests that the formation of **3** occurs via a concerted proton transfer mediated by bridging water molecules in the singlet ground state, leading directly from **1** to **3**. Indeed, a search for a corresponding transition state **13** was successful and yielded barriers of only 37 and 41.2 kJ/mol for concerted proton transfer mediated by two bridging water molecules (see the Supporting Information). Hence, **3** is directly obtained from **1** via transition state **13**, and intermediate **2** is not formed.

Once **3** is present, ring closure occurs, and species **4** is formed (Scheme 2). This process is exothermic by −61.3 kJ/mol and −97.2 kJ/mol at the DFT/B3LYP and SCS-MP2 levels, respectively. The computed energy barrier for this

Table 1. Relative Energies (in kJ/mol) of the Intermediate and Transition States in the Uncaging Reaction[a]

	DFT/B3LYP		SCS-MP2	
intermediate/TS	E_{rel} (kJ/mol)	f_B	E_{rel} (kJ/mol)	f_B
1 + H_2O	12.2	0.007	13.5	0.004
[**13** + $2H_2O$]$^{\#b}$	49.3		54.7	
2 + H_3O^+	156.4	0	156.9	0
3 + H_2O	0.0	99.993	0.0	99.996
[**34** + H_2O]$^{\#}$	61.9			
4 + H_2O	−61.3		−97.2	
[**47** + H_3O^+]$^{\#}$	4.3		−6.7	
7 + H_3O^+	−142.2		−148.5	

[a]All energies are given relative to *aci*-nitro intermediate **3**, the starting point of the uncaging process. [b]Barrier for concerted proton transfer mediated by two bridging water molecules (see the text).

dx.doi.org/10.1021/ja410594y | J. Am. Chem. Soc. 2014, 136, 3430–3438

process is 61.9 kJ/mol at the DFT/B3LYP level, leading to a computed Arrhenius rate constant of 1.75×10^{-11} s^{-1}. From intermediate **4**, the reaction is supposed to proceed via the deprotonated ring intermediate **5** toward acylal intermediate **6** and the nitroso product **7**, which eventually dimerizes.[21] However, the final dimerization is not considered here. Geometry optimizations of the deprotonated species **5** did not lead to a stable equilibrium structure, but instead, release of the caged acetate during the structure optimization was observed. This suggests strongly that the uncaging process proceeds via a concerted reaction involving deprotonation of the *aci*-nitro group, cleavage of the five-membered ring, and release of the acetate. A search of the potential energy surface for a corresponding transition state **47** connecting species **4** and **7** directly was successful (Figure 9), pinpointing the release of the caged acetate as a concerted reaction involving the simultaneous splitting of two bonds during deprotonation. At the DFT/B3LYP and SCS-MP2 levels of theory, the energy barrier along this concerted reaction amounts to 65.6 and 90.5 kJ/mol, respectively. The final product **7** and the protonated released compound are the energetically lowest compounds along the reaction path, lying 142.2 and 148.5 kJ/mol lower than the most stable *aci*-nitro intermediate **3** (Table 1). According to our calculations, the acylal intermediate **6** and the deprotonated species **5**, like the deprotonated *aci*-nitro intermediate **2**, are never formed during the uncaging reaction.

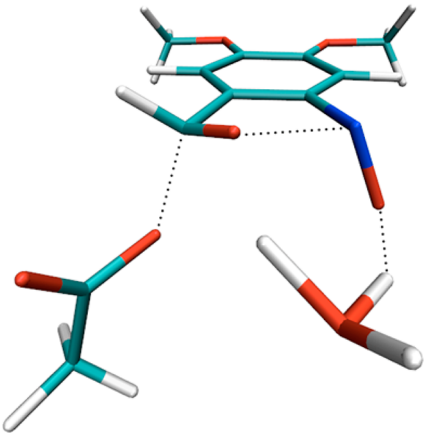

Figure 9. Structure of transition state **47** leading directly from intermediate **4** to the nitroso product **7** via a concerted deprotonation and breaking of two bonds.

DISCUSSION

The femtosecond transient absorption spectrum at long delay times in the UV/vis region reveals a spectral shape very similar to the one observed for a 4,5-methylenedioxynitrobenzyl compound 20 ns after excitation, for which the features were ascribed to the triplet/triplet absorption known to be the most dominant signal for these and DMNB compounds with lifetimes in the range of 700 ns in DMSO solution.[17] We assign the broad featureless absorption that dominates the whole spectral range directly after excitation to an excited state that either decays within 200 fs back to the ground state (as indicated by the 200 fs component at the position of the ground-state bleach) or undergoes ISC to form the *aci*-nitro intermediate $\mathbf{1}^3$, which has a weak absorption band around 530 nm and a stronger one around 410 nm. This is supported by the calculated spectra for this intermediate (Figure 4). Since these calculated spectra were estimated in the gas phase, a shift of a few tens of nanometers toward lower energies is likely. The intermediate $\mathbf{1}^3$ has a lifetime of about 3.6 ps and decays either by relaxation back to the ground state or reaction to form intermediate $\mathbf{3}^3$. The rise of the absorbance around 400 nm with that time constant can be explained by the recovery of the ground state that is spectrally superimposed on that absorbance. Another band rises around 500 nm, whereas the signal around 530 nm decays with 3.6 ps, which can be explained by a change from the $\mathbf{1}^3$ to the $\mathbf{3}^3$ absorption. This transition toward intermediate $\mathbf{3}^3$ is also in agreement with the quantum-chemical results, which showed that the lowest-energy absorption of intermediate $\mathbf{3}^3$ is about 25 nm lower than that of $\mathbf{1}^3$. Whether a reaction in the singlet state also takes place could not be verified from this measurement, since the triplet state is known to be the most dominant feature after excitation because of a high extinction coefficient and therefore might obscure the spectral contributions of the singlet absorption. As indicated by the calculated spectra, the spectral position of the most dominant signal in the singlet state should appear around 370 nm, which is superimposed with the ground-state bleach and the strong 410 nm band of the triplet state. Comparing the absorption change of the bleach signal directly after excitation with the one at 1 ns reveals a recovery of about 95% (see the Supporting Information). Since here also spectral features of the triplet absorption appear on top of the bleach signal, this roughly estimated yield can only provide an upper limit for the conversion efficiency into intermediate **3**, which then should be below 5%.

To obtain insight into the spectral features of the intermediate present at the maximum delay time in the infrared, a time slice taken after 1 ns was added to a scaled steady-state spectrum of NVOC. The spectrum of this intermediate present after 1 ns can be found in Figure 10.

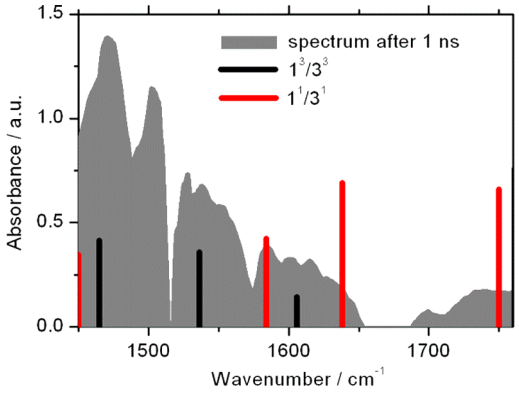

Figure 10. Estimated IR intermediate spectrum 1 ns after excitation. Here a scaled steady-state spectrum of pure NVOC was added to the DAS of the infinite time constant. In addition, calculated spectra of intermediates **1** and **3** in the singlet and triplet states are shown.

Since the calculated spectral features of intermediates **1** and **3** are very much alike, a distinction between them is ambiguous in the mid-IR. Furthermore, the reaction toward intermediate **3** takes place in a time range of 3.6 ps, and the formation of **3** is therefore obscured by the dominant cooling processes, which prevent direct observation of this process. In addition to the derived spectrum of the species present after 1 ns, the calculated spectra of the relevant intermediates are shown.

dx.doi.org/10.1021/ja410594y | J. Am. Chem. Soc. 2014, 136, 3430−3438

Scheme 3. Mechanism of the Photolysis of NVOC−Puromycin

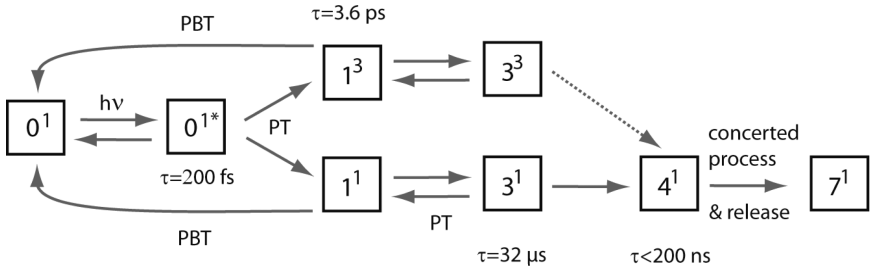

Remarkably, this absorption spectrum confirms the formation of the intermediate $\mathbf{1}^3/\mathbf{3}^3$ within the investigated time range. After the cooling processes that take place within 7.8 ps, indicating the *aci*-nitro form, the product features can be observed. In addition, the strong bleach signal around 1520 cm^{-1} indicates the loss of the nitro vibration upon protonation. It appears likely that intermediate $\mathbf{1}^1/\mathbf{3}^1$ is also present after 1 ns. This is supported by the width of the absorption band around 1600 cm^{-1}, where two singlet modes appear on the higher- and lower-energy sides of the only triplet mode in this spectral range. Furthermore, only the singlet form shows some contributions in the range above 1700 cm^{-1}, where the experimental spectrum also shows an absorption.

There are two arguments that explain the low uncaging efficiency of this compound. One is the lowering of the energy of the nonreactive triplet state with respect to the reactive one. Therefore, the molecules following the triplet pathway get trapped in this nonreactive state and do not contribute to the uncaging. The other argument is the in general low uncaging efficiency via the singlet state, since it competes with an efficient proton back-transfer reaction. The flash photolysis experiment showed that after 5 μs no contribution of the triplet absorption around 500 nm is left (Figure 5). Only the absorbance of the *aci*-nitro intermediate in the singlet state can be found, and this intermediate is most likely formed directly in the singlet state. Comparing the spectrum after 1 ms with the calculated nitroso spectrum reveals the accomplishment of the uncaging reaction. Intermediate **4**, which is formed by attack of the oxygen in the nitro group to the benzylic carbon atom, does not contribute in the investigated spectral range, as indicated by the calculated spectra. Experimentally this should lead to an absorption pattern where only the ground-state bleach can be observed. Since we did not observe this pattern in the flash photolysis experiment, it appears likely that a very fast decay of that intermediate that is well below the temporal resolution of the experiment (200 ns) occurs directly after its formation.

CONCLUSIONS

The photolysis reaction of NVOC−puromycin was studied by means of femtosecond transient absorption and flash photolysis measurements and quantum-chemical calculations. The photoreaction is different from the one observed for unsubstituted oNB compounds. Not only does the absorption spectrum appear to be bathochromically shifted by about 50 nm, but also, fewer intermediates are formed along the reaction pathway. Scheme 3 summarizes our results. After excitation of the NVOC, a fast proton transfer (PT) from the exocyclic carbon atom to the nitro group takes place to form the *aci*-nitro intermediate **1**, and although **1** could be detected only in the triplet manifold, the additional formation of the *aci*-nitro intermediate in the singlet manifold appears likely. In thermal equilibrium, the balance of the *aci*-nitro intermediates is highly on the side of intermediate **3**, which is formed by a proton transfer reaction mediated by water molecules, whereas the formation of intermediate **2** is rather unlikely because of its high relative energy of about 160 kJ/mol. Intermediate **3** decays on a 32 μs time scale via an exothermic process leading to intermediate **4**, which has a lifetime below 200 ns and therefore is not observed. This short lifetime can easily be explained by the low energy of the transition state connecting intermediates **4** and **7** (only 4.3 kJ/mol). As a result of that fact, the decay of intermediate **3** can be considered as the rate-limiting step of the uncaging process.

Our study sheds light on the molecular mechanism taking place after photoexcitation of NVOC. This provides a basis that allows further optimization of these valuable types of cages with respect to their quantum yields.

ASSOCIATED CONTENT

Supporting Information

Single transients and fits from the time-resolved measurements, the FTIR spectrum of the solvent, structures of the transition states, a single transient taken around 2340 cm^{-1}, and details of the synthesis of NVOC puromycin. This material is available free of charge via the Internet at http://pubs.acs.org.

AUTHOR INFORMATION

Corresponding Author

wveitl@theochem.uni-frankfurt.de

Notes

The authors declare no competing financial interest.

ACKNOWLEDGMENTS

We thank the Deutsche Forschungsgemeinschaft (DFG) for financial support through SFB 902 “Molecular Principles of RNA-Based Regulation”.

REFERENCES

(1) McCray, J. A.; Trentham, D. R. *Annu. Rev. Biophys. Biophys. Chem.* **1989**, *18*, 239.
(2) Adams, S. R.; Tsien, R. Y. *Annu. Rev. Physiol.* **1993**, *55*, 755.
(3) Giovannardi, S.; Lando, L.; Peres, A. *News Physiol. Sci.* **1998**, *13*, 251.
(4) Kaplan, J. H.; Forbush, B.; Hoffman, J. F. *Biochemistry* **1978**, *17*, 1929.
(5) Hoffmann, N. *Chem. Rev.* **2008**, *108*, 1052.
(6) Klán, P.; Šolomek, T.; Bochet, C. G.; Blanc, A.; Givens, R.; Rubina, M.; Popik, V.; Kostikov, A.; Wirz, J. *Chem. Rev.* **2013**, *113*, 119.
(7) Mayer, G.; Heckel, A. *Angew. Chem., Int. Ed.* **2006**, *45*, 4900.
(8) Ellis-Davies, G. C. R. *Nat. Methods* **2007**, *4*, 619.
(9) Lee, H.-M.; Larson, D. R.; Lawrence, D. S. *ACS Chem. Biol.* **2009**, *4*, 409.

(10) Bort, G.; Gallavardin, T.; Ogden, D.; Dalko, P. I. *Angew. Chem., Int. Ed.* **2013**, *52*, 4526.
(11) Bochet, C. G. *J. Chem. Soc., Perkin Trans. 1* **2002**, 125.
(12) Patchornik, A.; Amit, B.; Woodward, R. B. *J. Am. Chem. Soc.* **1970**, *92*, 6333.
(13) Cameron, J. F.; Fréchet, J. M. J. *J. Am. Chem. Soc.* **1991**, *113*, 4303.
(14) Ciamician, G.; Silber, P. *Ber. Dtsch. Chem. Ges.* **1901**, *34*, 2040.
(15) Barltrop, J. A.; Schofield, P. *Tetrahedron Lett.* **1962**, *3*, 697.
(16) Wettermark, G. *J. Phys. Chem.* **1962**, *66*, 2560.
(17) Bley, F.; Schaper, K.; Görner, H. *Photochem. Photobiol.* **2008**, *84*, 162.
(18) Schaper, K.; Mobarekeh, S. A. M.; Doro, P.; Maydt, D. *Photochem. Photobiol.* **2010**, *86*, 1247.
(19) Görner, H. *Photochem. Photobiol. Sci.* **2005**, *4*, 822.
(20) Aujard, I.; Benbrahim, C.; Gouget, M.; Ruel, O.; Baudin, J.-B.; Neveu, P.; Jullien, L. *Chem.—Eur. J.* **2006**, *12*, 6865.
(21) Schaper, K.; Etinski, M.; Fleig, T. *Photochem. Photobiol.* **2009**, *85*, 1075.
(22) Mewes, J. M.; Dreuw, A. *Phys. Chem. Chem. Phys.* **2013**, *15*, 6691.
(23) Solomek, T.; Mercier, S.; Bally, T.; Bochet, C. G. *Photochem. Photobiol. Sci.* **2012**, *11*, 548.
(24) Morris, A.; Favelukes, S.; Arlinghaus, R.; Schweet, R. *Biochem. Biophys. Res. Commun.* **1962**, *7*, 326.
(25) Yarmolinsky, M. B.; Haba, G. L. D. L. *Proc. Natl. Acad. Sci. U.S.A.* **1959**, *45*, 1721.
(26) Darken, M. A. *Pharmacol. Rev.* **1964**, *16*, 223.
(27) Hamm, P.; Kaindl, R. A.; Stenger, J. *Opt. Lett.* **2000**, *25*, 1798.
(28) Neese, F. *Wiley Interdiscip. Rev.: Comput. Mol. Sci.* **2012**, *2*, 73.
(29) Shao, Y.; Molnar, L. F.; Jung, Y.; Kussmann, J.; Ochsenfeld, C.; Brown, S. T.; Gilbert, A. T. B.; Slipchenko, L. V.; Levchenko, S. V.; O'Neill, D. P.; DiStasio, R. A.; Lochan, R. C.; Wang, T.; Beran, G. J. O.; Besley, N. A.; Herbert, J. M.; Lin, C. Y.; Van Voorhis, T.; Chien, S. H.; Sodt, A.; Steele, R. P.; Rassolov, V. A.; Maslen, P. E.; Korambath, P. P.; Adamson, R. D.; Austin, B.; Baker, J.; Byrd, E. F. C.; Dachsel, H.; Doerksen, R. J.; Dreuw, A.; Dunietz, B. D.; Dutoi, A. D.; Furlani, T. R.; Gwaltney, S. R.; Heyden, A.; Hirata, S.; Hsu, C.-P.; Kedziora, G.; Khalliulin, R. Z.; Klunzinger, P.; Lee, A. M.; Lee, M. S.; Liang, W.; Lotan, I.; Nair, N.; Peters, B.; Proynov, E. I.; Pieniazek, P. A.; Rhee, Y. M.; Ritchie, J.; Rosta, E.; Sherrill, C. D.; Simmonett, A. C.; Subotnik, J. E.; Woodcock, H. L.; Zhang, W.; Bell, A. T.; Chakraborty, A. K.; Chipman, D. M.; Keil, F. J.; Warshel, A.; Hehre, W. J.; Schaefer, H. F., III; Kong, J.; Krylov, A. I.; Gill, P. M. W.; Head-Gordon, M. *Phys. Chem. Chem. Phys.* **2006**, *8*, 3172.
(30) Parr, R. G.; Wang, W. *Int. J. Quantum Chem.* **1989**, *47*, 101.
(31) Becke, A. D. *J. Chem. Phys.* **1993**, *98*, 1372.
(32) Grimme, S. *J. Chem. Phys.* **2003**, *118*, 9095.
(33) Møller, C.; Plesset, M. S. *Phys. Rev.* **1934**, *46*, 618.
(34) Eichkorn, K.; Treutler, O.; Ohm, H.; Haser, M.; Ahlrichs, R. *Chem. Phys. Lett.* **1995**, *240*, 283.
(35) Schäfer, A.; Klamt, A.; Sattel, D.; Lohrenz, J. C. W.; Eckert, F. *Phys. Chem. Chem. Phys.* **2000**, *2*, 2187.
(36) Dreuw, A.; Head-Gordon, M. *Chem. Rev.* **2005**, *105*, 4009.
(37) Neumann, K.; Verhoefen, M.-K.; Mewes, J.-M.; Dreuw, A.; Wachtveitl, J. *Phys. Chem. Chem. Phys.* **2011**, *13*, 17367.
(38) Mewes, J.-M.; Neumann, K.; Verhoefen, M.-K.; Wille, G.; Wachtveitl, J.; Dreuw, A. *ChemPhysChem* **2011**, *12*, 2077.
(39) Mewes, J.-M.; Pepler, E.; Wachtveitl, J.; Dreuw, A. *J. Phys. Chem. A* **2012**, *116*, 11846.
(40) Ho, J.; Coote, M. *Theor. Chem. Acc.* **2010**, *125*, 3.